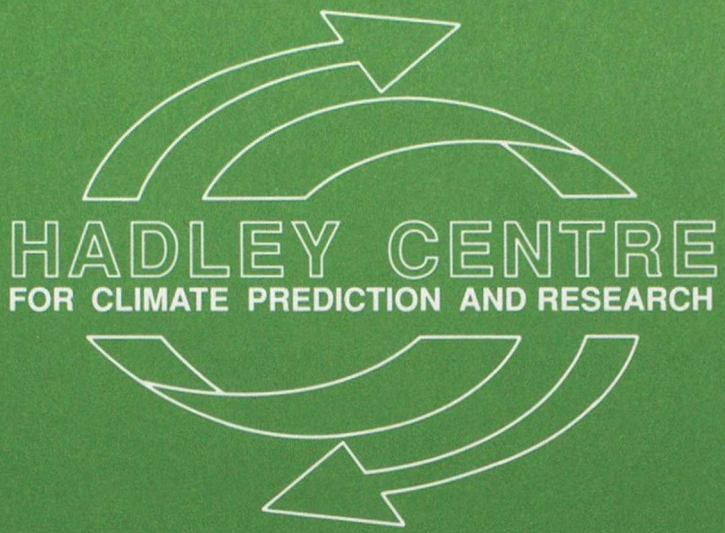

A tropic-wide oscillation of boreal summer rainfall and patterns of sea-surface temperature

by

M N Ward, K Maskell, C K Folland, D P Rowell and R Washington

CRTN 48

June 1994

CLIMATE
RESEARCH
TECHNICAL
NOTE

Hadley Centre
Meteorological Office
London Road
Bracknell
Berkshire RG12 2SY

A TROPIC-WIDE OSCILLATION OF BOREAL SUMMER RAINFALL AND PATTERNS OF SEA-SURFACE TEMPERATURE

M.N. Ward, K. Maskell, C.K. Folland, D.P. Rowell and R. Washington

Summary

We present observational and numerical modelling evidence of a tropic-wide teleconnection pattern in July to September which links the monsoon regions of Central America, North Africa and India with atmospheric variability in the tropical western Pacific. Some of these individual relationships have been identified by previous authors analysing historical data: the Sahel and India[1,2]; the Sahel and Caribbean[3,4]; Sahel/India and Indonesia[5,6]. However, we suggest here that these relationships are part of a coherent mode, encompassing much of the boreal summer tropics. The mode may be an important component of climate variation in the tropics on timescales from the interannual to millennia. Here, we particularly study the mode on timescales of the Southern Oscillation. We identify two types of central/east tropical Pacific warm events and cold events. TYPE I events have a strong contrast in sea-surface temperature anomalies between the central/eastern tropical Pacific and western tropical Pacific, leading to a strong perturbation in the longitude of the maximum in the zonal sea-surface temperature profile at 0-10°S in the western Pacific. These events are associated with a near-global rainfall teleconnection pattern which includes the tropic-wide oscillation described above and also links with rainfall over (eastern) Australia, western Europe, North America, South America and southern Africa. TYPE II events have large sea-surface temperature anomalies in the central/eastern tropical Pacific, but anomalies in the western Pacific are much weaker than in TYPE I events and the longitude of the maximum of SST at 0-10°S in the western Pacific is not greatly perturbed from its mean position. These events are associated with a much more limited rainfall teleconnection pattern. So sea-surface temperature anomalies associated with TYPE I events seem to trigger the tropic-wide oscillation. These results clearly follow on from much previous work on the Southern Oscillation and its global teleconnections, pioneered by such researchers as Walker and Bliss[7] and Troup[8]. Here, however, we offer a different interpretation of some of these teleconnections. We suggest that they are part of a tropic-wide oscillation that is a naturally recurring pattern of atmospheric variability, which certain types of Pacific warm events and cold events can trigger. On longer timescales, the oscillation might be triggered by interhemispheric changes in sea-surface temperatures, and we present some evidence for this during the present century.

1. Introduction

Variability of the tropical (40°N to 20°S) atmosphere in July to September (JAS) has been investigated using (a) observed land station rainfall data, interpolated to grid-boxes using a method similar to Hulme[9], but developed to increase data coverage (Hulme[10]) and (b) simulated rainfall in 20 atmospheric general circulation model (GCM) experiments. All data were placed on a 5°lat x 15°long grid for analysis. The observed rainfall data given to us by Hulme were on a 2.5°lat x 3.75°long grid; any interpolations of missing station data to produce this dataset were made by averaging the monthly percentage rainfall anomalies reported by nearby stations[9]. Then, to place the rainfall data on the 5°lat x 15°long grid, we averaged the JAS rainfall anomalies in all available constituent 2.5°lat x 3.75°long grid-boxes.

The GCM experiments used one of the earlier versions of the UK Met. Office model[11,12] with 11 vertical levels (using sigma co-ordinates) and a horizontal resolution of 2.5°lat x 3.75°long. The GCM was forced with global sea-surface temperatures (SSTs) from April to October taken from the UK Met. Office Historical SST dataset[13] for each of the years 1949, 50, 58, 76, 83, 84, 87, 88, 89, 90, which provide a good sample of tropical variability in recent decades. Two GCM experiments were run for each year from different initial atmospheric conditions: (a) starting from the UK Met. Office analysis for 26 March 1984 (experiment set GLO84) and (b) for 31 March 1987 (experiment set GLO87)[14]. Previous papers[14,15,16] have shown that the model simulates the interannual variability of rainfall over the Sahel of Africa with very good skill, and rainfall over India with moderate skill.

2. Tropical Rainfall EOFs

The principal pattern of rainfall anomaly variation in the observed and GCM tropical rainfall data has been estimated by calculating the first correlation eigenvector (EOF) of each dataset[17]. The GCM and observed patterns (Fig. 1), while differing in details of precise location, show marked broad-scale similarity by linking rainfall anomalies in the monsoon regions of Central America, North Africa and India. Some of the individual associations have been previously noted using observed data[1-4]. The GCM and observed patterns (Fig. 1) also have some similarity in the western Pacific, with increased rainfall near Indonesia and decreased rainfall near the Philippines being positively correlated with rainfall in the boreal summer monsoon regions. Again, some of these individual associations have been previously noted in observed data[5,6]. The GCM EOF has a very clear north-south dipole in the western Pacific. In the observed EOF, this dipole is rotated about 30° clockwise and is weaker. However, the broad-scale tropic-wide agreement leads us to argue that the GCM and observed EOFs are describing the same large-scale phenomenon. For

brevity, we subsequently refer to this phenomenon as the tropic-wide oscillation (TO). In support of our result, the first EOF of global station precipitation data for June to August 1901-80 found by Lau and Sheu[18] is similar in pattern to the EOFs in Fig. 1. However, their EOF was more concentrated in the tropical Pacific, and their interpretation was solely in terms of warm events/cold events in the tropical Pacific. Here, we offer a different interpretation, suggesting that the TO is a natural recurring pattern of atmospheric variability, which certain types of Pacific warm events and cold events can trigger (see sections 4-10 below).

3. Simulated and Observed Time Coefficients of Rainfall EOF1

Method

We have assessed whether the GCM, forced by the observed SST, is simulating the TO correctly in each modelled year. The strength and phase of the TO in the JAS observed (z_o) and modelled (z_m) rainfall anomalies has been measured by calculating the amplitude (or "time coefficient") of the GCM EOF1 pattern:

$$z_{mi} = \sum_{j=1}^{n} w_j \, r_{mij}$$

$$z_{oi} = \sum_{j=1}^{n} w_j \, r_{oij}$$

where i indicates year, r_{mij} and r_{oij} are the JAS modelled and observed rainfall anomalies (in standardised units) for grid box j in year i, and w_j is the GCM EOF1 weight for grid-box j. The summation is performed using only those grid-boxes with observed data, and only those grid-boxes where $\mathrm{mod}(w_j)>0.4$. The aim is to compare the strength of a base rainfall anomaly pattern in (i) the observed rainfall data, and (ii) the rainfall data simulated by the GCM. Thus it makes sense to compare observed and modelled data using the same base pattern (here chosen to be the GCM EOF1 pattern) measured over the same grid-boxes (thus boxes with no observed data must be rejected). The constraint $\mathrm{mod}(w_j)>0.4$ was introduced to concentrate verification on the most significant regions of the TO, and to remove noise. This ensures modelled and observed rainfall are compared using just the main centres of the EOF, excluding regions with low weights, which are most likely representing chance random statistical associations in the data. (Results have been found to be largely insensitive to varying the threshold value of 0.4.)

Results

There is good agreement between the relative changes in values of z_m and z_o, though variation in z_o is considerably less (Fig. 2, correlation of z_m and z_o is 0.76 using GLO84 experiments for z_m and 0.71 using GLO87, both significant at the 2.5% level). So when the GCM is forced with observed SST, it skilfully simulates the relative changes in the observed TO. Some of the reduced variability in z_o is expected since we are using the GCM EOF pattern which was calculated to maximize the variance of z_m, not z_o. A further reason for the higher variance of z_m is probably that this particular GCM was over-sensitive to SST forcing.

Also noteworthy in Fig. 2 is the near-perfect agreement between the GLO84 and GLO87 time-series of z_m (correlation, r=0.97), showing that the interannual variability of the TO in the GCM is insensitive to initial atmospheric conditions, and that the TO variability between experiments results almost entirely from the differences in the SST forcing.

4. Two Types of Pacific Warm Events and Cold Events

Previous studies[19,20] have found a link between Pacific warm events (cold events) and below (above) normal rainfall in the Sahel of Africa and India. In this section we investigate if there are two types of Pacific warm events/cold events: Type I that modulate Sahel and Indian rainfall and Type II that do not.

For this, we have analysed 1904-90 time-series of JAS rainfall totals (in mean standardised anomaly units) for the Sahel and for India[21] and a time-series measuring the strength of Pacific warm events and cold events in JAS (time coefficients of global SST EOF2[22,6]). Each series was high-pass filtered using an integrated random walk smoothing algorithm[23,24]. The 50% cut-off amplitude was set to 11.25 years, so the dominant timescales of the Southern Oscillation (SO) are in the high-pass filtered data. The high pass filter is only really important for the Sahel rainfall series, whose strong multi-decadal variability makes study of shorter period variability difficult without filtering.

We have sub-divided our data (see Table 1) into two sets: (a) years when there is a warm event phase (cold event phase) in the Pacific (determined by whether SST EOF2 was above or below normal), AND Sahel and Indian rainfall are BOTH below (above) normal - these are FIT years, i.e. they fit the relationships between the SO and Sahel/Indian rainfall identified by Ropelewski and Halpert[19,20]; (b) all other years - these are NOT FIT years.

We want to know if the warm events/cold events in the FIT years have any notable differences from those in the NOT FIT years. To identify this, we could calculate a composite SST difference for extreme warm events MINUS cold events for (i) those years in the FIT category and (ii) those years in the NOT FIT category. Instead, we have calculated the correlation between SST EOF2 and each 10°lat x 10°long SST time-series in (i) FIT years and (ii) NOT FIT years. This produces a result similar to the compositing approach - one way to view the result is as a standardised composite difference for warm event phase MINUS cold event phase in which each year has been given a different weight based on the magnitude of the anomalies in that particular year. (When calculating correlations, little weight is given to years of small anomalies, and most weight is given to extremes, so inclusion of near normal years in the analysis is not a great problem since the technique naturally gives most weight to the extreme years).

The correlation of SST EOF2 and 10°lat x 10°long SST in FIT years 1951-90 (Fig. 3a) suggests that warm events/cold events in these years (TYPE I) are characterised by a strong contrast in SST anomaly between the central/eastern tropical Pacific and the western equatorial Pacific, extending south through the region of the South Pacific Convergence Zone. When the correlation analysis is repeated for the NOT FIT years (Fig. 3b), over much of the central and eastern tropical Pacific the pattern is very similar to that in FIT years (Fig. 3a). While there are some differences between Figs. 3a and 3b in the Atlantic and Indian Oceans, we focus on the differences in the western Pacific, since the overlying local atmosphere is very sensitive to SST in this region (see next section). In Fig. 3b, the correlations in the western Pacific are reduced, and the switch from statistically significant positive correlations to negative correlations at 0-10°S takes an extra 10° of longitude compared to FIT years (Fig. 3a), suggesting warm events and cold events in TYPE II years have large SST anomalies in the central/eastern tropical Pacific, but do not have such a sharp and substantial transition to opposite SST anomalies in the western Pacific, with the difference between TYPE I and TYPE II particularly strong at 0-10°S.

To check the reproducibility of the result in the first half of the century, the analysis has been repeated using data for 1904-50. Once again, the FIT correlation map (Fig. 3c) has strong negative correlations in the southwestern tropical Pacific, whereas the NOT FIT map (Fig. 3d) has much weaker correlations in this region. Averaged over the equatorial and southwestern tropical Pacific (the box marked on Fig. 3a), the mean correlation for FIT and NOT FIT is -0.56 and -0.28 after 1950 (Figs. 3a,b), and -0.49 and -0.19 before 1950 (Fig. 3c,d). For the box centred at 5°S 155°E, the difference in correlation is particularly marked: -0.84 v -0.27 after 1950 and -0.92 v -0.43 before 1950.

Table 1 also shows that the fraction of FIT years compared to NOT FIT years may vary with time. For example, the fraction of FIT years is higher after 1950 than before 1950.

It has been suggested that SST data in the western Pacific may not be sufficiently reliable prior to 1950 to detect interannual climate variability[25]. One indirect check of the data reliability is to calculate the correlation between a given SST time-series, and SST in all other grid-boxes. Note that the data used here have no spatial smoothing across grid-boxes. So if the data have a very low signal to noise ratio, then the correlation of adjacent grid-boxes will fall. Using the JAS SST time-series at 5°S, 155°E as the base series, correlation maps for the years 1904-50 (Fig. 4a) and 1951-90 (Fig. 4b) are very similar in the western Pacific, suggesting little degradation of data for this region in the earlier years. Furthermore, the signal to noise ratio must be quite good to achieve correlations >0.7 for adjacent grid-boxes.

5. SST and Near-surface Divergence in the Western and Central Tropical Pacific

Direct forcing of the near-surface atmosphere by SST will lead to a close association between patterns of near-surface divergence and SST in the absence of other forcing[26]. This section studies the relationship between SST and near-surface divergence in the western Pacific, since a direct response of the atmosphere to SST in this region is an important link in the chain connecting TYPE I warm events/cold events to the TO.

To study near-surface divergence, we have used a divergence dataset calculated from trimmed monthly mean 2°lat x 2°long COADS near-surface wind data[27]. The wind data were placed on a 10°lat x 10°long grid using anomalies, following the method outlined in Ward[6,21]. Trends in the wind data were also corrected using surface pressure gradients prior to the calculation of a 10°lat x 10°long near-surface divergence dataset 1949-88, using finite differences of the seasonal mean vector wind anomalies[21].

The first JAS SST EOF 1949-88 (Fig. 5a) in the tropical western Pacific is an east-west dipole pattern. In the west, the largest weights are at 0-10°S. The pattern for 1904-90 is very similar (Fig. 5b).

The first JAS divergence EOF (Fig. 5c) has a more complicated pattern. Over the equatorial latitudes 10°N-10°S it is also an east-west dipole. Again, largest weights in the west are at 0-10°S. In the west, the pattern is also a north-south dipole, with large positive weights centred at 0-10°S and large negative weights at 10-20°N. (Also, in the east, the weights at 10-20°N and at 10-20°S have a sign that is opposite

to the weights at 10°S-10°N.)

The correlation between the time-coefficients of SST EOF1 and divergence EOF1 is extremely high (Fig. 5d). So we suggest that, in the region of the EOF analysis, the Equatorial atmosphere is responding directly to the SST, especially at 0-10°S in the western Pacific. One hypothesis is that equatorial regions of enhanced near-surface convergence lead to a zone of diabatic heating anomaly (enhanced penetrative convection leading to enhanced latent heating), which leads to descent and near-surface divergence anomalies about 10° latitude polewards, which is consistent with the meridional overturning found by Gill[28] in response to a line of heating in the tropical atmosphere. These ideas are supported by the local correlation between near-surface divergence and near-surface SST[21], which is strongly negative in these equatorial SST regions, but actually positive and statistically significant at 10-20°N in the western Pacific. It is, however, possible to get such a positive local correlation between SST and near-surface divergence and for the model of Lindzen and Nigam[26] to still hold perfectly well. So the precise physical mechanisms for the connection between divergence EOF1 and SST EOF1 require further analysis, but the strong physical connection between the two EOF patterns is difficult to refute given the very high correlation of their time coefficients (Fig. 5d).

6. The Zonal Profile of Western Pacific SST at 0-10°S

The results in sections 4 and 5 suggest SST at 0-10°S in the western Pacific is particularly important for local and remote atmospheric patterns in JAS. The climatological SST maximum actually resides north of the Equator in JAS, so at first one might have expected this to be the most important region, but there are a number of possible reasons why the atmosphere should be so sensitive to the SST at 0-10°S. Firstly, the zonal SST profile at 0-10°S contains strong gradients with a strong maximum in the western Pacific, whereas the profiles north of the Equator are much flatter. Also, the standard deviation of SST anomalies at 0-10°S in the western Pacific is much higher than that north of the Equator. Thus anomalies at 0-10°S will exert a strong control on the anomalous SST gradients in the region, which in turn are believed to often control near-surface atmospheric divergence[26]. Finally, near-surface winds that blow across the region 0-10°S in the western Pacific are an important source for the near-surface convergence north of the Equator in the China Sea.

To further support the above ideas, we present the mean zonal SST profiles for 0-10°S across the equatorial Pacific and eastern Indian Ocean that are associated with warm events TYPE I and II and cold

events TYPE I and II respectively (Fig. 6). For these mean profiles, only years associated with distinct El Niño or La Niña events were used[29,30] (years in bold italics in Table 1). The SST maximum is located at different longitudes in each profile: 155°E for cold event I, 165°E for cold event II, 175°E for warm event II and 175°W for warm event I. A further difference between TYPE I and TYPE II warm events is the colder SST westwards from 155°E in the TYPE I profile. In the cold event profiles, TYPE I has a much sharper and slightly higher SST maximum than TYPE II. Fu *et al.*[31] analysed a number of El Niño SST patterns in the equatorial Pacific and distinguished types similar to our I and II based on the location of the SST maximum, the extent of SST>28.5°C, and the SST anomalies in the western Pacific. Current understanding[26,32] suggests that convection in the overlying tropical atmosphere is highly sensitive to quite small variations in the magnitude and position of SST maxima like those shown in Fig. 6.

7. Rainfall Teleconnections Associated with the Two Types of Pacific Events

The above results suggest that the zonal profile of SST at 0-10°S in JAS is an important factor in atmospheric patterns in JAS. We have therefore studied the zonal SST profile in each year 1950-90, and categorised years according to the longitude of the SST maximum in the western Pacific (Table 2, SST data prior to 1950 were not sufficiently complete to define the SST maximum). In this way we are defining TYPE I (FIT) and TYPE II (NOT FIT) years purely in relation to SST, and this is indicated by a subscript s in the following text. Years in which the SST maximum is shifted west of 160°E define cold phase TYPE I_s years, while years in which the maximum is east of the dateline define warm phase TYPE I_s. Years in which the SST maximum lies between these two longitudes define warm and cold phase years TYPE II_s.

The analysis now follows the same principles applied in the calculation of Fig. 3, but using grid-box rainfall instead of SST. We correlate SST EOF2 with grid-box rainfall in TYPE I_s years (Fig. 7a) and TYPE II_s years (Fig. 7b). The correlation map for TYPE I_s years shows that these warm events/cold events are associated with an almost global-scale teleconnection pattern, including the TO seen in the observed and GCM rainfall EOF patterns (Fig. 1) and also large correlations over western Europe (positive r over Iberia and Mediterranean, negative r over northwestern Europe) and North America (positive r over western USA, negative r over northwestern Canada) in the Northern Hemisphere, and in the Southern Hemisphere over Australia, especially eastern districts (negative r), South America (negative r in the North, positive r in the South) and southern Africa (positive r). In all, 24.9% of the correlations in Fig. 7a are statistically significant at the 5% level.

TYPE II_s events, as identified by the NOT FIT_s years, have a geographically more limited influence that covers parts of the tropical Pacific (as far as can be studied) and northern South America (Fig. 7b). Only 6.4% of all correlations in Fig. 7b are significant at the 5% level. So usually only TYPE I_s events trigger the TO, which we conclude is the source of at least some of the association between the SO and Sahel/Indian rainfall. Distinction between TYPE I_s and TYPE II_s events in the boreal spring of each year should lead to improved seasonal forecasting for the regions which the TO connects (Fig. 7a). However, analysis of the GCM results and empirical data (not shown here) suggests that the TO can be triggered by SSTs other than those associated with warm/cold events in the Pacific, so maximum skill in predicting the TO is likely through consideration of the global SST field. Nonetheless, we do suggest that the TO is particularly sensitive to the zonal profile of SST at 0-10°S in the western Pacific.

8. The Tropic-wide Oscillation on Longer Timescales

There is evidence that the TO has been a mode of tropical climate variation on longer timescales as well, which would be consistent with the original work of Kraus[1,2] which was concerned with the multi-decadal timescale association of rainfall in tropical North Africa and India. There is evidence[21], based on analysis of ocean-atmosphere datasets and rainfall datasets, for the presence of the TO through much of the tropics in the climate fluctuation that was most clearly marked by the onset of Sahelian drought around 1968. A similar climate fluctuation occurred in North Africa around 1900[1,33] and Fu and Fletcher[34] describe synchronous changes at that time in Indian monsoon rainfall and western Pacific circulation. Both the fluctuations around 1968 and 1900 accompanied changes in the mean SST of the Northern Hemisphere relative to the Southern Hemisphere (i.e. a change in the interhemispheric SST contrast). A relatively warmer Southern Hemisphere (including all the Indian Ocean) accompanies relatively drier conditions in the Sahel[22,35]. To show the relationship between interhemispheric contrast in SST and the TO, we have calculated the cross-spectrum between JAS values of SST EOF3[22,6] (time-series describing interhemispheric SST variations) and the time-series of the observed tropical rainfall EOF1 (Fig. 1b). For this, a rainfall EOF1 time-series was calculated for the full period of data used in this paper (1904-90) by projecting all available observed JAS rainfall anomalies for each JAS season onto the EOF in Fig. 1b. The 1904-90 cross-spectrum (Fig. 8) shows very high values of coherence squared for low frequency timescales, especially for periods greater than about 20 years, supporting the idea that the TO is related to the interhemispheric contrast in SST anomaly on multi-decadal timescales.

Finally, paleoclimatic data support the idea of synchronous droughts and wet periods in the boreal

summer monsoon regions on timescales of millennia[36], with a suggestion of interhemispheric changes in SST consistent with the multi-decadal variations seen over the last 100 years. So the TO may be an important component of climate variation in the tropics on timescales from the interannual to millennia, with various possible triggers, of which TYPE I warm events and cold events are but one.

Changes in the frequency of preferred atmospheric low frequency modes such as the Pacific North American pattern and the North Atlantic Oscillation are viewed as potentially important components of the atmosphere's response to increases in greenhouse gases. Likewise, the TO may be seen as a possible component of the tropical atmosphere's boreal summer response to future increases in greenhouse gases.

9. Simulation of the Tropic-wide Oscillation using SST EOFs

This paper has discussed a tropic-wide pattern of rainfall anomalies. The pattern has been related to Pacific warm events / cold events, and it has been suggested that the pattern can be best simulated by considering the SST in the western Pacific, along with the large-scale state of the El Niño / La Niña phenomenon. A further predictor of the TO has been suggested to be interhemispheric contrast in SST. We now make a first attempt at quantifying these relationships by performing a multiple regression over 1904-90 using time coefficients of JAS tropical rainfall EOF1 (TO, Fig. 1b) as the dependent variable and using as independent variables the JAS time coefficients of (a) SST EOF1 in the tropical western Pacific (WP1, Fig. 5b), (b) Global SST EOF2 (G2) and (c) Global SST EOF3 (G3). (Note that degrees of freedom is not reduced by serial correlation since the lag 1 autocorrelation of the TO is not statistically significant, r_1=0.04). Each series was standardised to have mean zero and standard deviation 1 over 1904-90, so the magnitude of the coefficients reflects the relative contribution of each independent variable to the model. The regression model is:

Multiple Regression Equation: TO = 0.45*WP1 - 0.33*G2 - 0.30*G3

Using a t-test, each term is very highly statistically significant (at <0.1% level), and the multiple correlation for the model is 0.82. The value of the TO simulated by the model in each year is plotted in Fig. 9, along with the observed value, showing that a large fraction of the observed TO variability can be simulated by the three SST patterns.

A further important technical point is that the residuals of the model after entering WP1 and G2 do not have significant serial correlation. Thus the entry of G3 into the model at this stage is not seriously affected by reduced degrees of freedom.

10. GCM Atmospheric Variability Associated with the Tropic-wide Oscillation

We conclude with some pointers to possible mechanisms of the mode in the GCM. Large-scale vertical ascent through the depth of the troposphere is closely associated with rainfall because rising air cools adiabatically until water condenses to form clouds. The release of latent heat upon condensation further fuels the ascent, and forms an important heating source that affects the local and remote tropical atmosphere[28]. Conversely, sinking air warms adiabatically and is able to hold more water in gaseous form, making rainfall unlikely. We have analysed the patterns of vertical motion in the GCM that are associated with the TO. Inspection of the model's tropical rainfall EOF1 (Fig. 1a) suggests that we should contrast atmospheric circulation in the western Pacific and atmospheric circulation over all other longitudes. So climatological vertical motion (based on the ten GLO84 experiments) has been calculated for the average of all longitudes away from the western Pacific (Fig. 10a) and in the western Pacific (Fig. 10b). Then, averaging over the same two longitudinal blocks, the difference in vertical motion was calculated for the three most negative modelled TO years MINUS the three most positive TO years (1950, 58, 88 MINUS 1983, 84, 87). To identify the years in the composite, the sign and magnitude of the TO in each year was measured using values of z_m calculated using the whole of the model EOF1 pattern (so the values of z_m are not exactly the same as those shown in Fig. 2, which was produced to verify the GCM against observations). In the composite difference for the block of longitudes away from the western Pacific, vertical motion near 15°N strengthens and shifts slightly north (Fig. 10c and 10a). Over the western Pacific, the changes are of opposite sign and larger in magnitude (Fig. 10d) and represent shifts in the dominance of the two climatological centres of ascent near 15°N and just south of the Equator (Fig. 10b).

In the tropics, strong ascent is often forced by regions of high SST, and especially SST maxima[26,32]. In the negative phase of the TO, there is strong ascent just south of the Equator in the western Pacific (inferred from the correlations with observed rainfall in Fig. 7a, and seen in the GCM in Fig. 10d). In cold events TYPE I, this is precisely the region of a sharp SST maximum in the zonal SST profile (Fig. 6), so there is evidence for a direct SST forcing of this part of the TO.

For warm events TYPE I, which we argued could trigger the positive TO phase, the SST maximum in the zonal SST profile at 0-10°S is well away from the western Pacific (Fig. 6). This profile also shows strong negative SST anomalies at 0-10°S in the western Pacific, which we associate with the anomalous descent that occurs just south of the Equator in the western Pacific in the TO positive phase (Fig. 10d).

The composite differences (Fig. 10c-d) mainly reflect changes in north-south overturning of the tropical atmosphere, as the east-west changes are small (not shown). We suggest that anomalous ascent and associated diabatic heating near the Equator in the western Pacific (Fig. 10d) may be inducing the opposite response near 15°N to the north[21], which would be broadly consistent with forced motion found in simple models of the tropical atmosphere[28]. In an earlier paper[15], it was also suggested that there were years when anomalous ascent in the region near 15°N in the China Sea seemed to be the source of forcing, with the equatorial pole acting as slave to the positive diabatic heating anomalies at 15°N. However, the SST and near-surface divergence analyses presented earlier suggest that it is the SST variability centred at 0-10°S that usually initially determines whether near-surface convergence will be concentrated in the southern pole near the Equator or in the northern pole at 15°N.

One interpretation of these results is that a compensation occurs between the anomalous, mainly north-south overturning over the western Pacific and the opposite anomalous north-south overturning found at most other longitudes. The compensation may be needed to maintain the climatological function (i.e. poleward heat and momentum transport) of the zonally averaged north-south overturning. This and other possible mechanisms are under investigation.

REFERENCES

1. Kraus, E.B. *Nature* **181,** 666-668 (1958).
2. Kraus, E.B. *Mon. Wea. Rev.* **105,** 1009-1018 (1977).
3. Hastenrath, S. *J. Atmos. Sci.* **33,** 202-215 (1976).
4. Hastenrath, S. *J. Atmos. Sci.* **35,** 2222-2231 (1978).
5. Meehl, G.A. *Mon. Wea. Rev.* **115,** 27-50 (1987).
6. Ward, M.N. *J. Climate* **5,** 454-475 (1992).
7. Walker, G.T. & Bliss, E.W. *Memoirs of the Royal Meteorological Society* **4,** 53-84 (1932).
8. Troup, A.J. *Quart. J. Roy. Meteor. Soc.* **91,** 490-506 (1965).
9. Hulme, M. *Climate Dyn.* **7,** 57-72 (1992).
10. Hulme, M. in *Global Precipitation and Climate Change* (eds Debois, M. & Desalmand, F.) (Springer Verlag, in press).
11. Slingo, A. *Dynamical Climatology Technical Note No. 29* (Met. Office, Bracknell, 1985).
12. Cunnington, W.M. & Rowntree, P.R. *J. Atmos. Sci.* **34,** 1366-1385 (1986).
13. Bottomley, M. *et al. Global Ocean Surface Temperature Atlas (GOSTA)*. pp20 and 313 Plates (HMSO, London, 1990).
14. Rowell, D.P. *et al. Geophys. Res. Let.* **19 (9),** 905-908 (1992).
15. Rowell, D.P. in *WCRP-68 WMO/TD No. 470* 145-151 (WMO, Geneva, 1991).
16. Rowell, D.P., Folland, C.K., Maskell, K. & Ward, M.N. *Quart. J. Roy. Meteor. Soc.* (accepted).
17. Jolliffe, I.T. *Principal Component Analysis* (Springer-Verlag, Berlin, 1986).
18. Lau, K.-M. & Sheu, P.J. in *Teleconnections Linking Worldwide Climate Anomalies* (eds Glantz, M.H., Katz, R.W. & Nicholls N.) 227-256 (Cambridge University Press, Cambridge, 1991).
19. Ropelewski, C.F. & Halpert, M.S. *Mon. Wea. Rev.* **115,** 1606-1626 (1987).
20. Ropelewski, C.F. & Halpert, M.S. *J. Climate* **2,** 268-284 (1989).
21. Ward, M.N. *Tropical North African Rainfall and Worldwide Monthly to Multi-decadal Climate Variations*. pp313 (PhD thesis, Reading University, 1994).
22. Folland, C.K., Owen, J.A., Ward M.N. & Colman A.W. *J Forecasting* **10,** 21-56 (1991).
23. Ng, C.N. & Young, P.C. *J Forecasting* **9,** 173-204 (1990).
24. Young, P.C., Ng, N., Lane, K. & Parker D.E. *J. Forecasting* **10,** 57-89 (1991).
25. Trenberth, K.E., Christy, J.R. & Hurrell, J.W. *J. Climate* **5,** 1405-1423 (1992).
26. Lindzen, R.S. & Nigam, S. *J. Atmos. Sci.* **44,** 2418-2436 (1987).

27. Woodruffe, S.D., Slutz, R.J., Jenne, R.L. & Steurer, P.M. *Bull. Amer. Meteor. Soc.* **68** 1239-1250 (1987).

28. Gill, A.E. *Quart. J. Roy. Meteor. Soc.* **106**, 447-462 (1980).

29. Diaz, H.F. & Kiladis, G.N. in *El Niño - Historical and Paleoclimatic Aspects of the Southern Oscillation* (Eds Diaz, H.F. and Markgraf, V.) 7-28 (Cambridge University Press, Cambridge, 1992)

30. Cayan, D.R. & Webb, R.H. in *El Niño - Historical and Paleoclimatic Aspects of the Southern Oscillation* (Eds Diaz, H.F. and Markgraf, V.) 29-68 (Cambridge University Press, Cambridge, 1992)

31. Fu, C., Diaz, H.F. & Fletcher, J.O. *Mon. Wea. Rev.* **114,** 1716-1738 (1986).

32. Gadgil, S.C., Joseph, P.V. & Joshi, N.V. *Nature* **312** 141-143 (1984).

33. Nicholson, S.E. in *The Sahara and The Nile* (eds Williams, M.A.J. and Faure, H.) 173-200 (A.A. Balkema, Rotterdam, 1980).

34. Fu, C. & Fletcher, J.O. *Beijing Advances in Atmospheric Sciences* **5,** 389-404 (1988).

35. Folland, C.K., Palmer, T.N. & Parker, D.E. *Nature* **320,** 602-607 (1986).

36. Street-Perrott, F.A. & Perrott, R.A. *Nature* **343,** 607-612 (1990).

ACKNOWLEDGEMENTS. Dr. Mike Hulme (Climatic Research Unit, Norwich, UK) kindly provided the observed rainfall data under UK DoE Contract PECD 7/12/78. The ideas in this paper have benefitted from discussions with Professor Brian Hoskins (University of Reading, UK) and from recent helpful comments made by Drs. Bob Livezey, Mike Davey and Serge Janicot, and by three referees.

TABLE 1 Classification of FIT and NOT FIT boreal summers, 1904-90. Wet = rainfall anomaly positive, Dry = rainfall anomaly negative. All series were high-pass filtered (50% cut-off amplitude = 11.25 years) prior to analysis. SST EOF2[22,6] measures the strength of El Niño/La Niña. A year is in bold if it is categorised as La Niña (row 1 and 3) or El Niño (row 2 and 4) by either Diaz and Kiladis[29] or Cayan and Webb[30]. The years in bold are used to produce the mean zonal SST profiles in Fig. 6 for La Niña TYPE I (row 1), El Niño TYPE I (row 2), La Niña TYPE II (row 3) and El Niño TYPE II (row 4).

FIT or NOT FIT	CRITERIA	JULY-SEPTEMBER SEASONS
FIT	Sahel and India Wet, SST EOF2 negative (La Niña phase)	***1906,09***,10,14,***16,24,50,54***,56,59,61,62,***64***, 67,***70,74,75***,78,81,***88***
	Sahel and India Dry, SST EOF2 positive (El Niño phase)	***1904***,05,07,***11,13,25,41***,48,***51,57,63,66***,68, ***72,76,77***,79,***82,87***
NOT FIT	Sahel or India Dry, SST EOF2 negative (La Niña phase)	***1908,17,20,21***,22,27,***28***,33,34,37,***38,39,42***, ***43***,45,46,***49,55***,60,***71,73***,80,84,85,***89***
	Sahel or India Wet, SST EOF2 positive (El Niño phase)	***1912,15,18,19,23,26***,29,***30,31,32***,35,36,***40***, 44,***47,52,53,58,65,69,83,86,90***

TABLE 2 Classification of FIT_s (TYPE I_s) and NOT FIT_s (TYPE II_s) boreal summers, 1950-90. Based on the longitude of the maximum in the zonal SST profile at 0-10°S in western Pacific.
(1970 not classified due to clear double SST maximum, 1952,53 not classified due to SST data missing in key grid-boxes).

FIT_s or NOT FIT_s	Longitude of SST maximum	JULY-SEPTEMBER SEASONS
FIT_s	Maximum west of 160°E	1950,54,62,64,75,78,81,88
	Maximum east of dateline	1951,57,60,65,72,76,77,82,87
NOT FIT_s	Maximum 160-170°E	1955,56,59,61,63,66,67,68,69,73,74,79,83, 84,85,89
	Maximum 170°E to dateline	1958,71,80,86,90

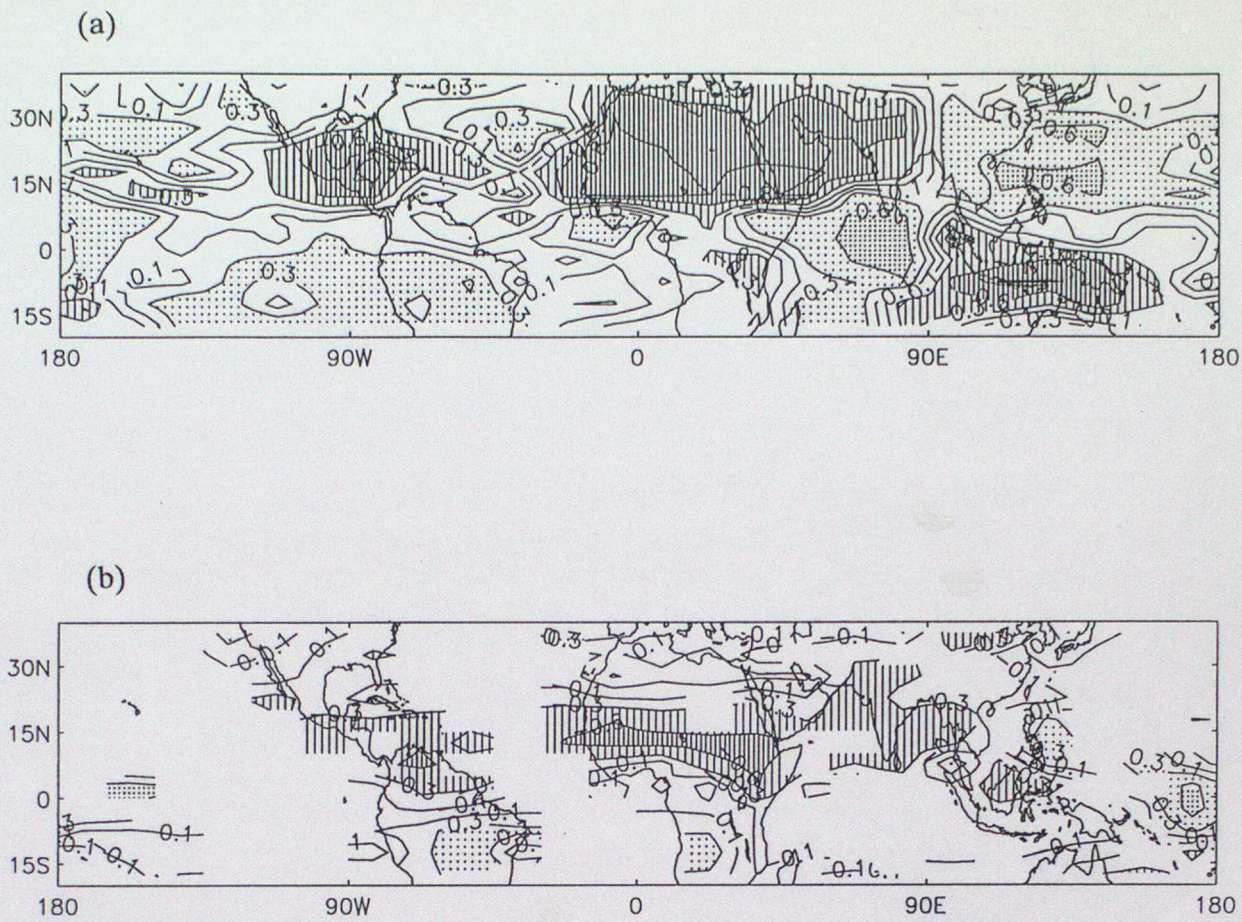

FIG. 1 The principal mode of July-September (JAS) rainfall variation 40°N to 20°S in (a) GCM simulations and (b) observed data, as estimated using a correlation eigenvector (EOF) analysis. (a) EOF1 pattern (explaining 25% of the total variance in the dataset) for GCM simulated rainfall from 20 experiments (10 GLO84 and 10 GLO87, see text). (b) EOF1 pattern for observed rainfall, 1949-90 (explaining 10% of total variance). Contours for both patterns at +/-.1,.3,.6,.8, shaded above .30, hatched below -.30. In (b), regions with insufficient data for analysis are not contoured. All rainfall data were interpolated to 5°lat x 15°long grid-box averages. The units of the EOF patterns are scaled so that the value for any grid-box is the correlation of the EOF time coefficients with all JAS rainfall values for that grid-box.

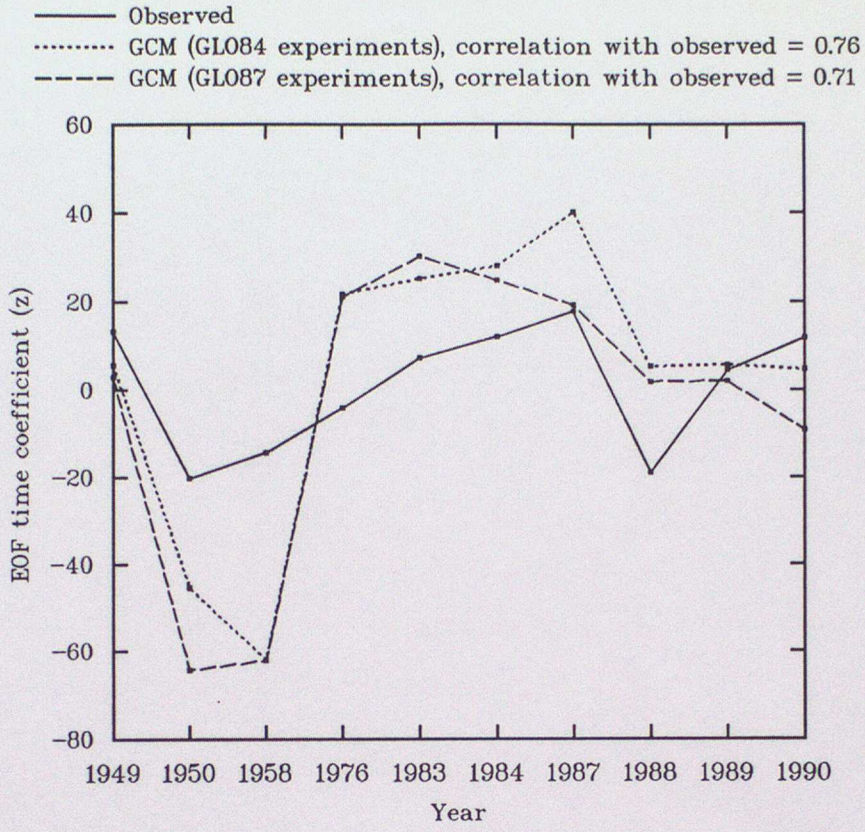

FIG. 2 Time coefficients of GCM EOF1 using GLO84 GCM data (short dash line), GLO87 GCM data (long dash line) and observed data (solid line) for each year that was modelled. (See text for details of time coefficient calculation).

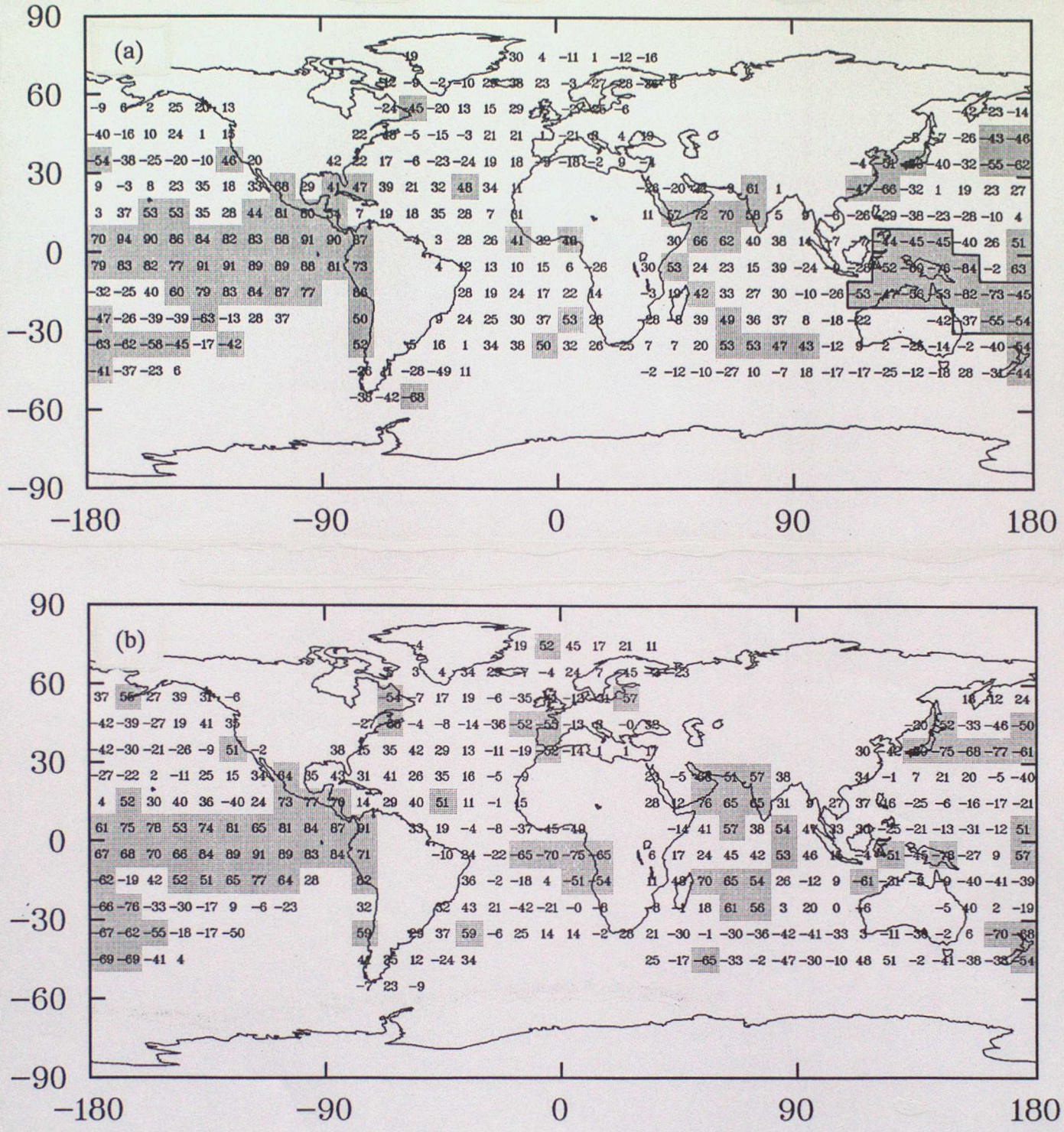

FIG. 3 (a) Correlation of global sea-surface temperature EOF2 time coefficients (measuring the strength of Pacific warm events/cold events) in JAS and JAS 10°lat x 10°long SST in FIT years 1951-90 (see Table 1), (b) Same as (a) but in NOT FIT years 1951-90. All series were high-pass filtered prior to analysis (passing timescales <11.25 years). Correlations locally significant at the 5% level are shaded. Regions with insufficient data for analysis are left blank on the maps.

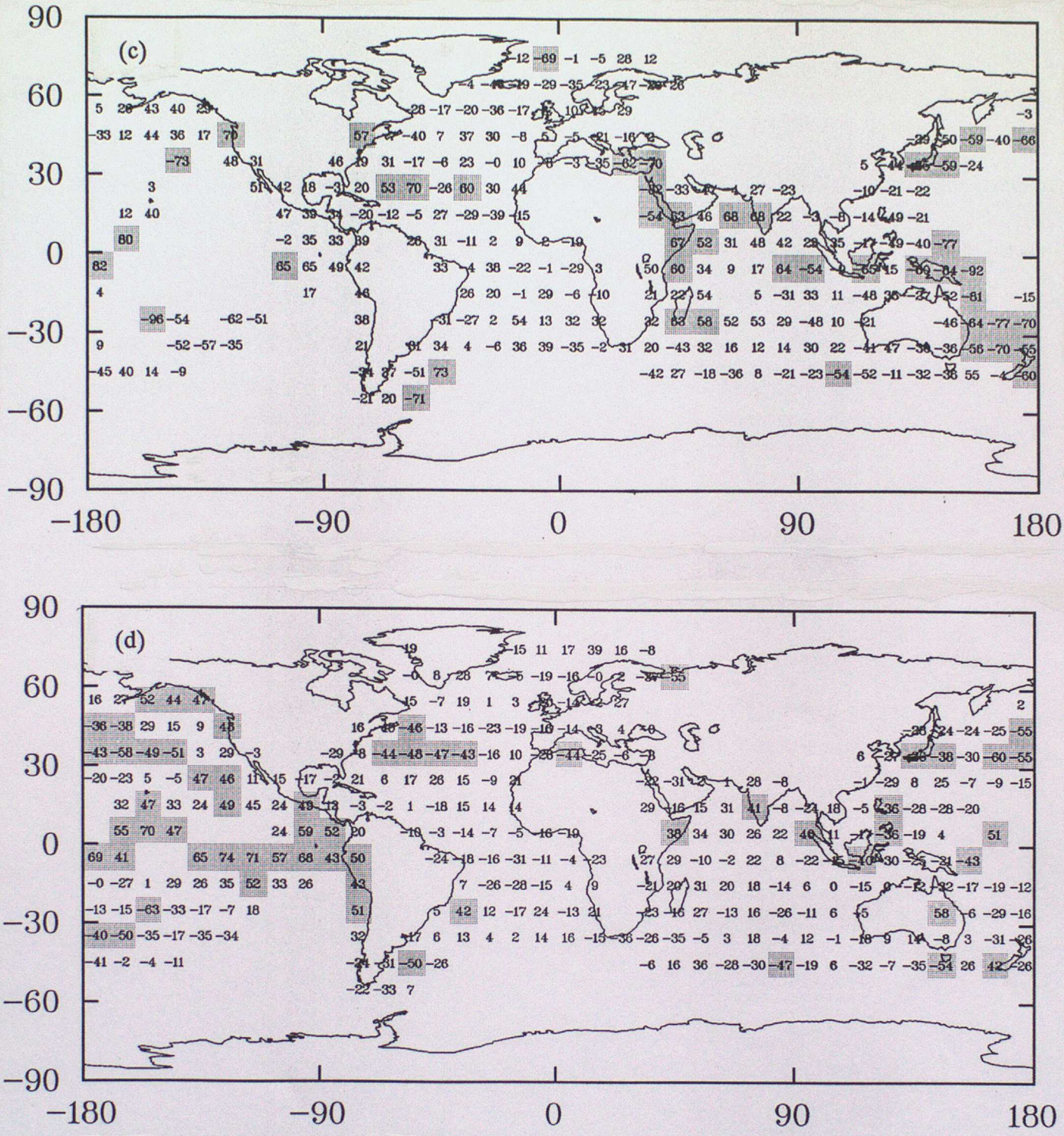

FIG. 3 (continued) (c) Same as (a) but in FIT years 1904-50, (d) Same as (a) but in NOT FIT years 1904-50.

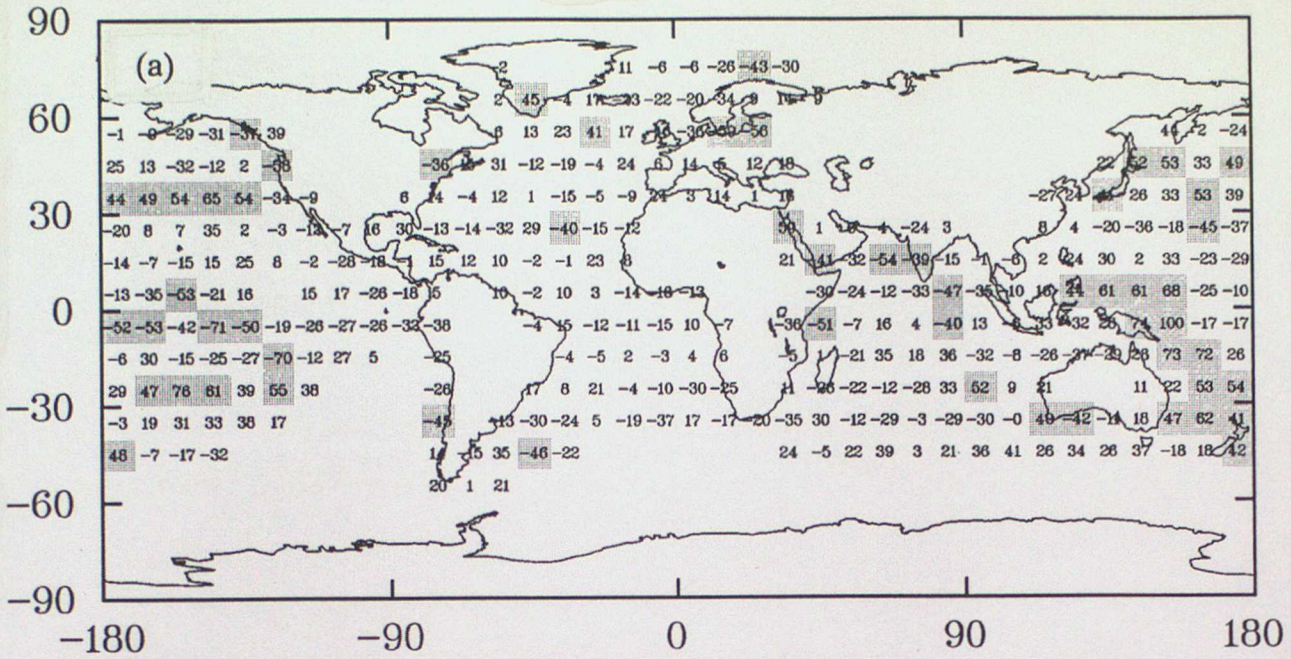

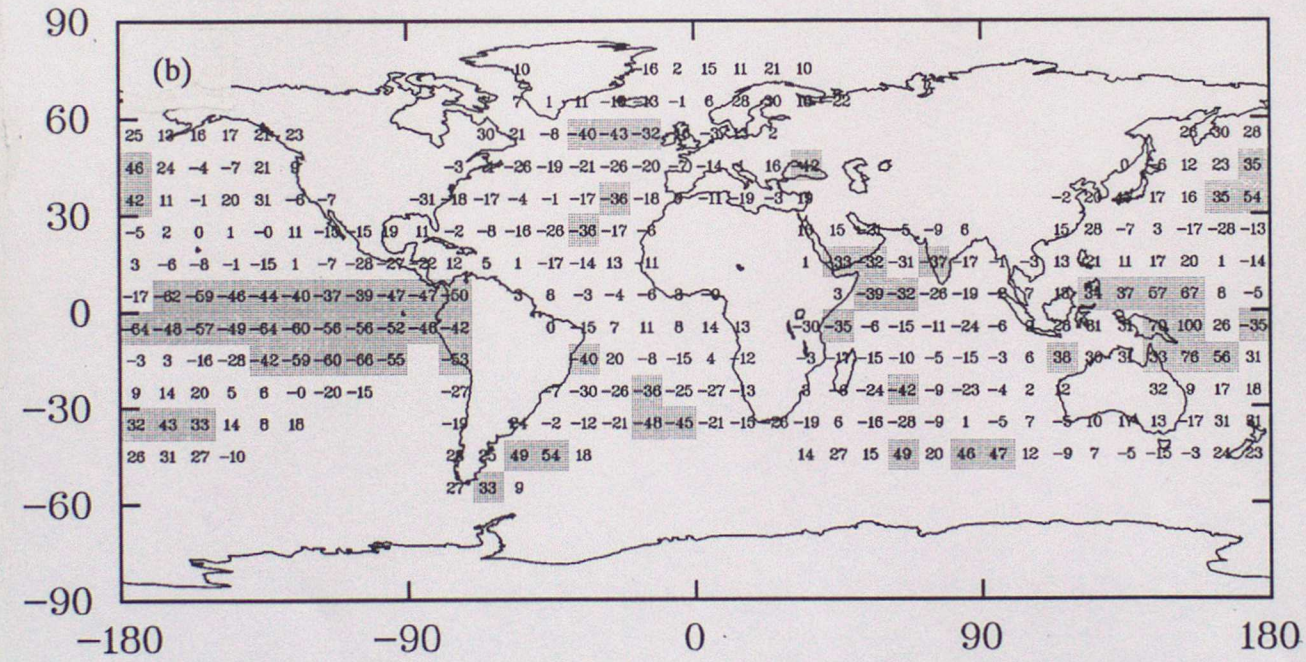

FIG. 4 Correlation between 10°lat x 10°long SST anomaly grid-box time-series centred 5°S, 155°E, and each available 10°lat x 10°long SST anomaly time-series for the world ocean (a) 1904-50, (b) 1951-90. Correlations locally significant at the 5% level are shaded. All series were high-pass filtered prior to analysis (passing timescales <11.25 years). A map using unfiltered data (not shown) is almost identical in the western Pacific region.

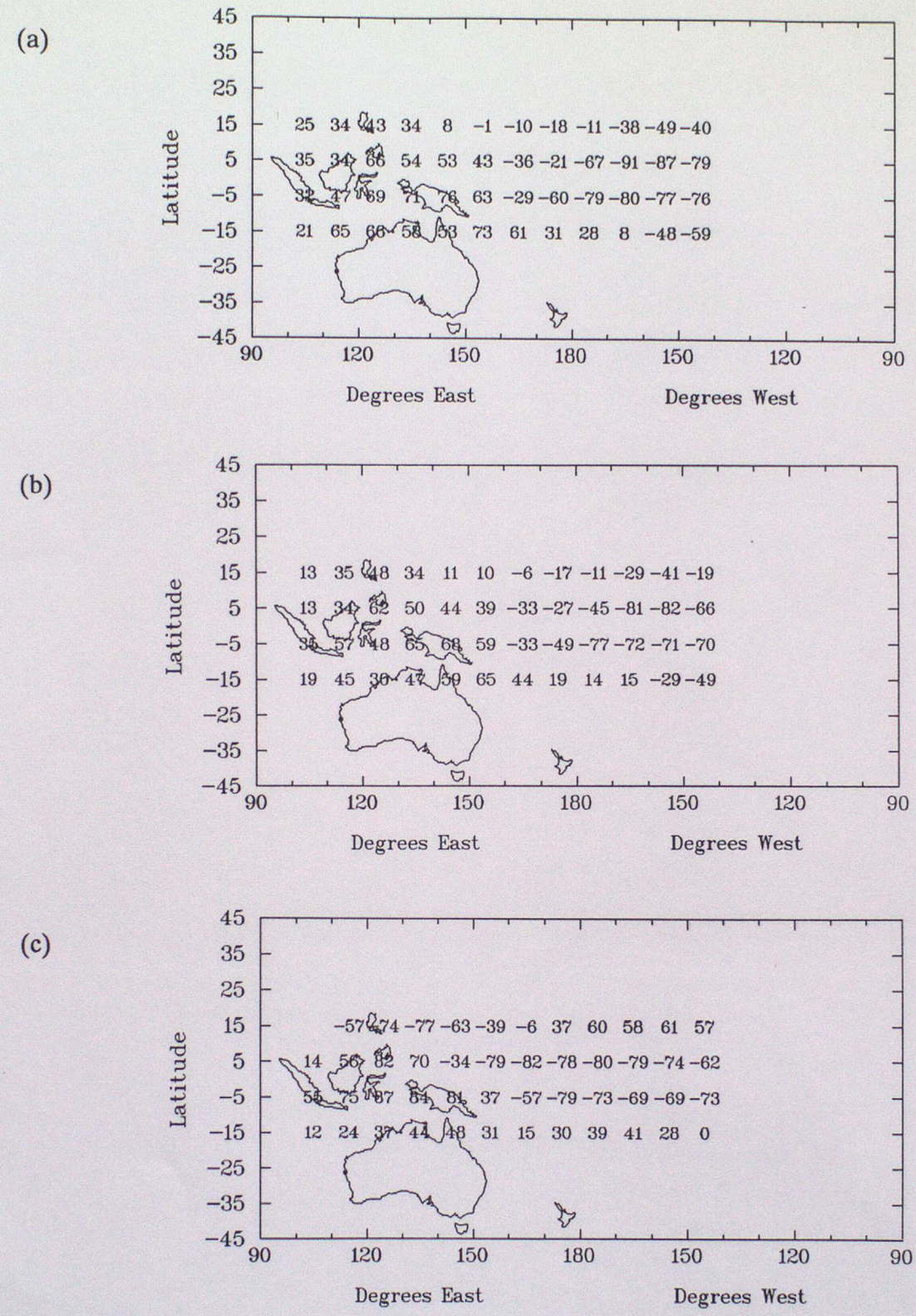

FIG. 5 (a) First correlation EOF 1949-88 for 10°lat x 10°long JAS SST anomalies in the tropical central and western Pacific (28.6% of total variance). (b) Same as (a) but for 1904-90 (21.6% of total variance). (c) Same as (a) but for near-surface divergence 1949-88 (35.2% of total variance). All series were high-pass filtered prior to analysis (passing timescales <11.25 years).

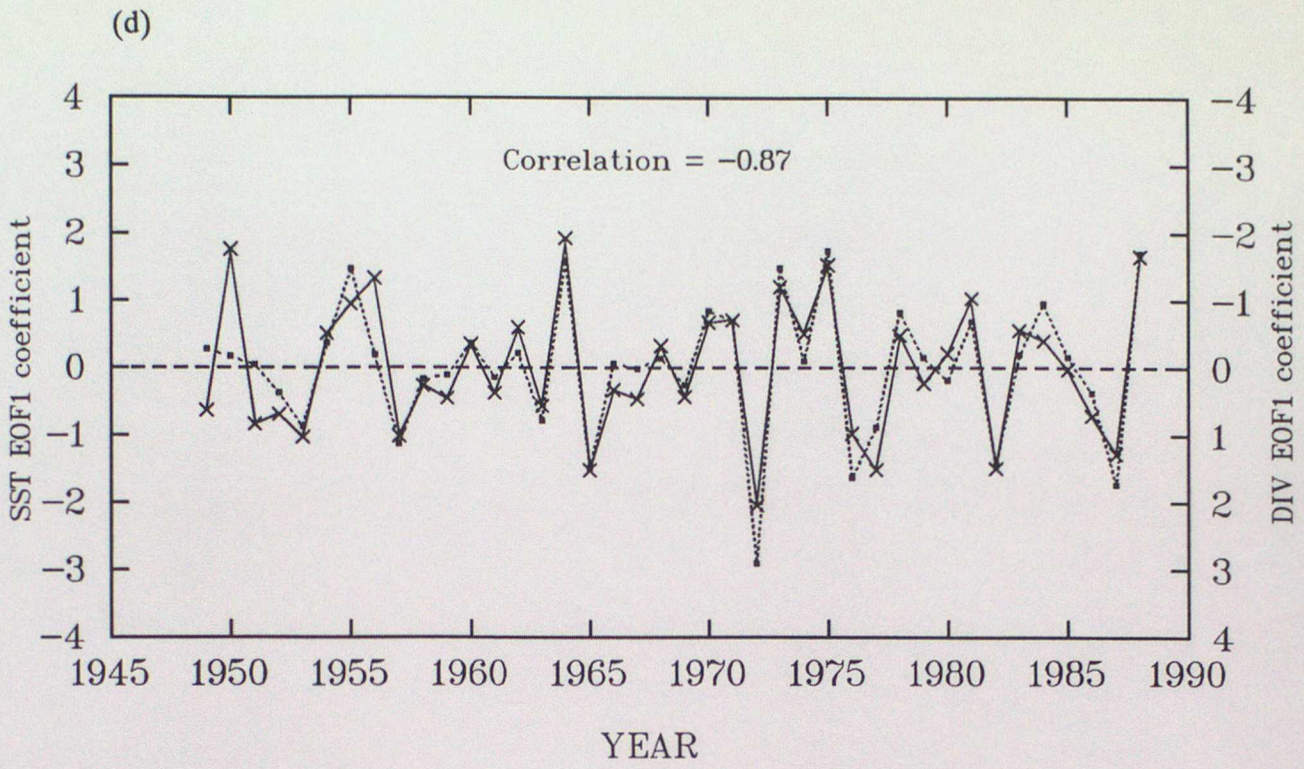

FIG. 5 (continued) (d) Observed JAS time coefficients 1949-88 of tropical central and western Pacific SST EOF1 in Fig. 5a (solid line with crosses) and near-surface divergence EOF1 in Fig. 5c (dashed line).

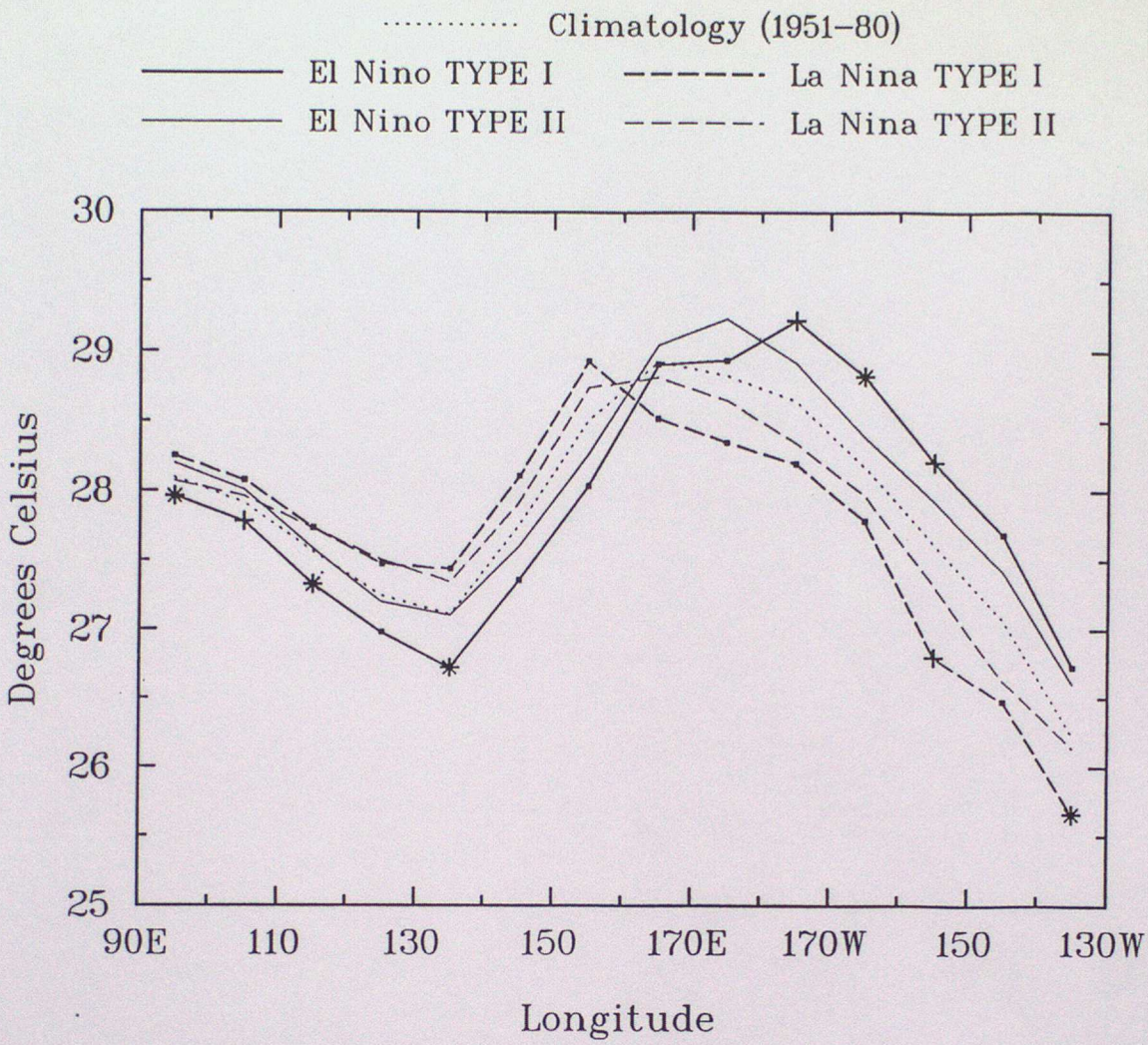

FIG. 6 Mean zonal SST profiles at 0-10°S from the eastern Indian Ocean to the central Pacific for El Niño and La Niña TYPE I and TYPE II. The years that contribute to each profile are in italics in Table 1. On the El Niño TYPE I curve, an asterisk (cross) indicates a 10°lat x 10°long mean value that is significantly different at the 5% (10%) level from the corresponding El Niño TYPE II value. Likewise, symbols on the La Niña TYPE I curve test the difference between La Niña TYPE I and TYPE II. All series were high-pass filtered prior to analysis (passing timescales <11.25 years). The filtered values (which are effectively anomalies from a climatology appropriate to each time-point) were added to 1951-80 climatological values to form the actual plotted profiles.

(a)

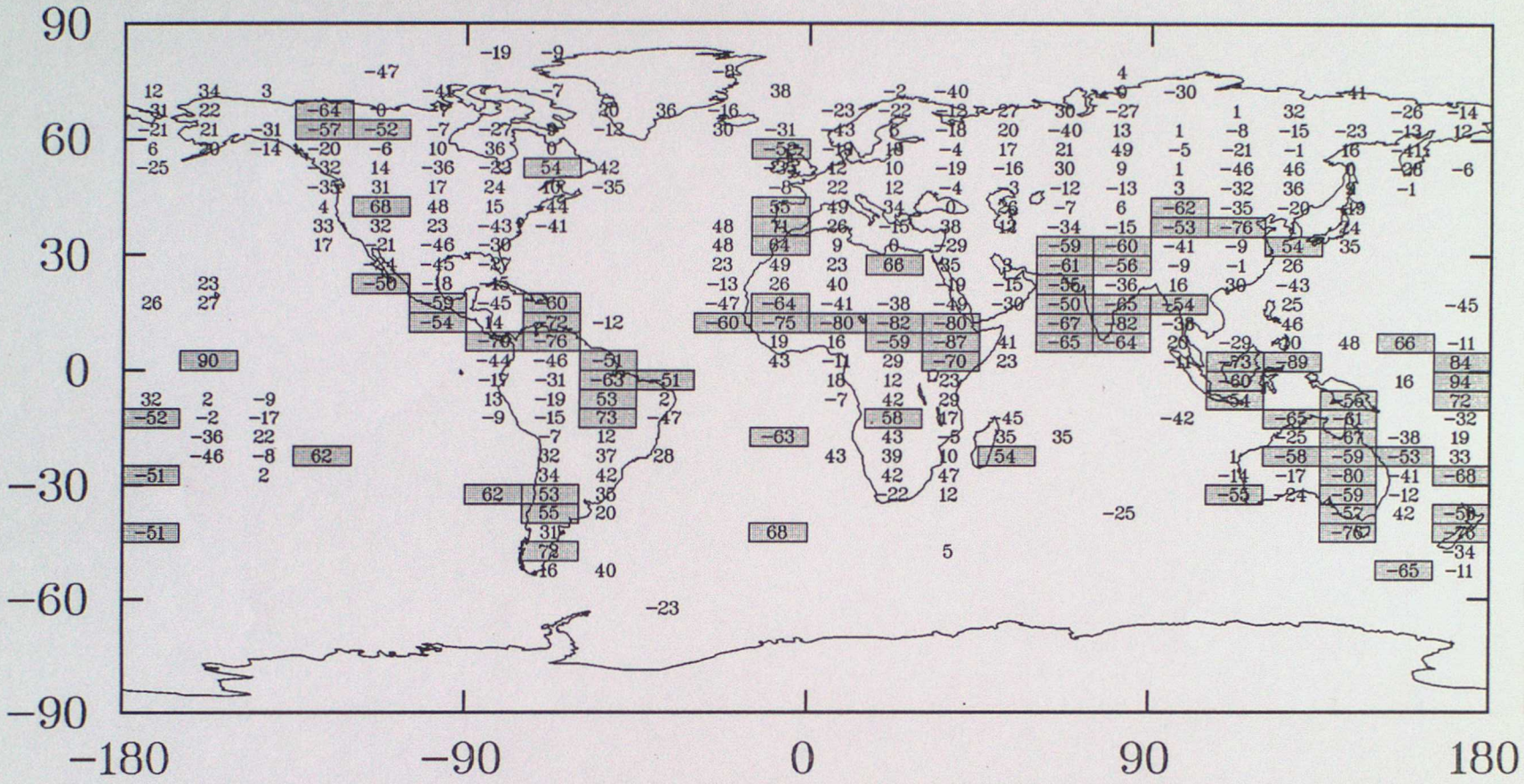

FIG. 7 (a) Correlation of global sea-surface temperature EOF2 time coefficients in JAS and JAS 5°lat x 15°long rainfall in FIT_s years 1950-90 (see Table 2). Correlations locally significant at the 5% level are shaded and boxed. All series were high-pass filtered prior to analysis (passing timescales <11.25 years).

(b)

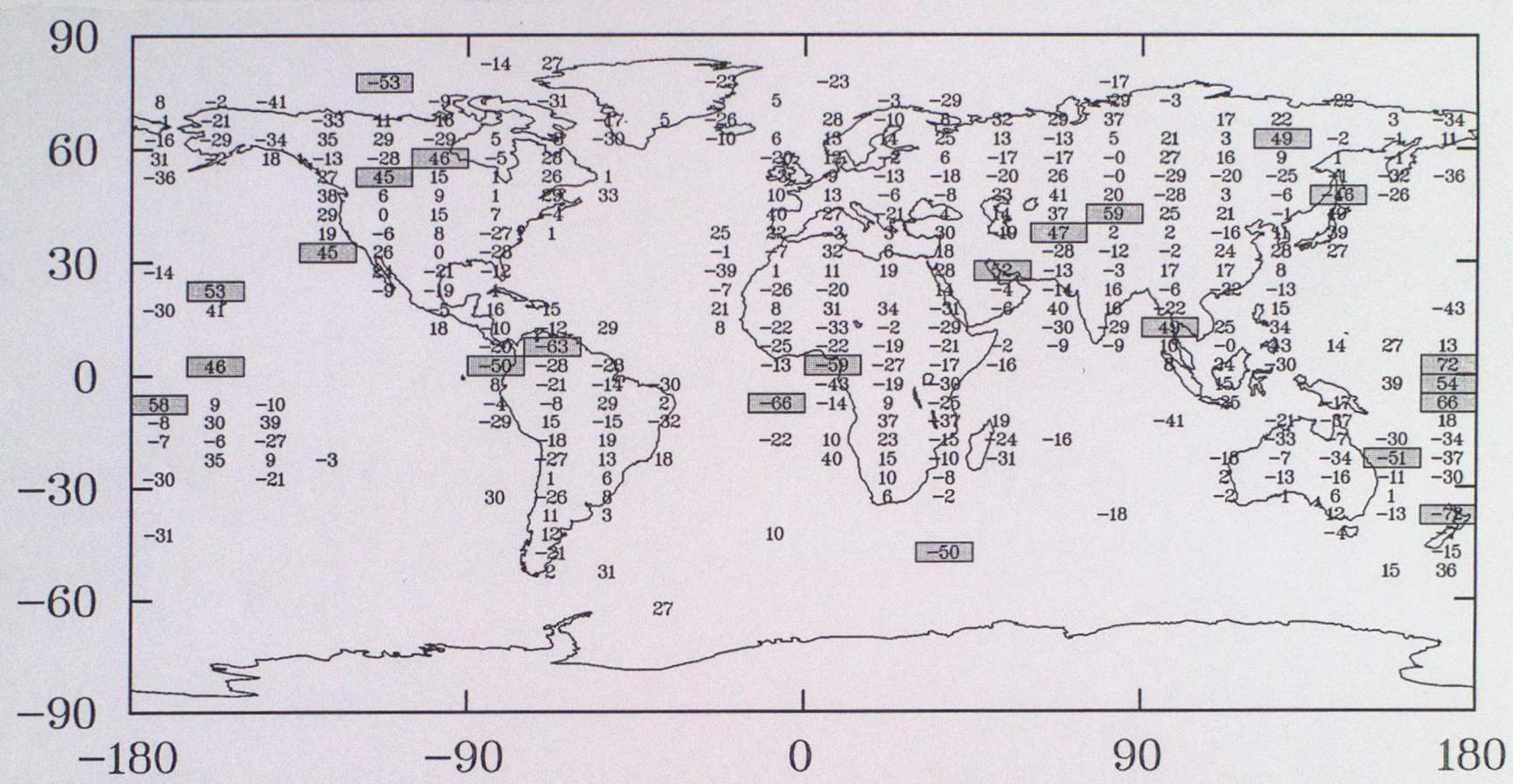

FIG. 7 (continued) (b) Same as (a) but in NOT FIT$_s$ years.

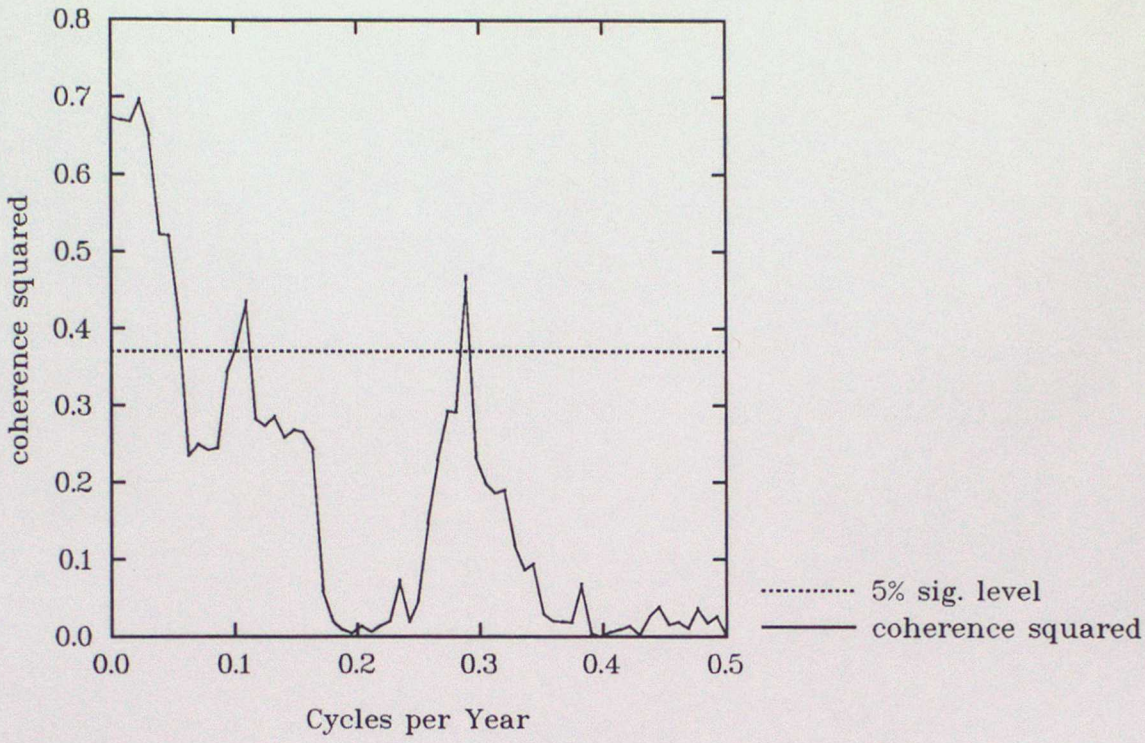

FIG. 8 Cross spectrum 1904-90 between JAS values of global SST EOF3^{22,6} (representing interhemispheric SST anomaly contrast) and tropical rainfall EOF1 (Fig. 1b, representing the tropic-wide oscillation). Time-series are linearly detrended prior to analysis. The coherence squared is calculated using a Fast Fourier Transform, smoothing the coefficients to yield about 15 degrees of freedom in each spectral estimate.

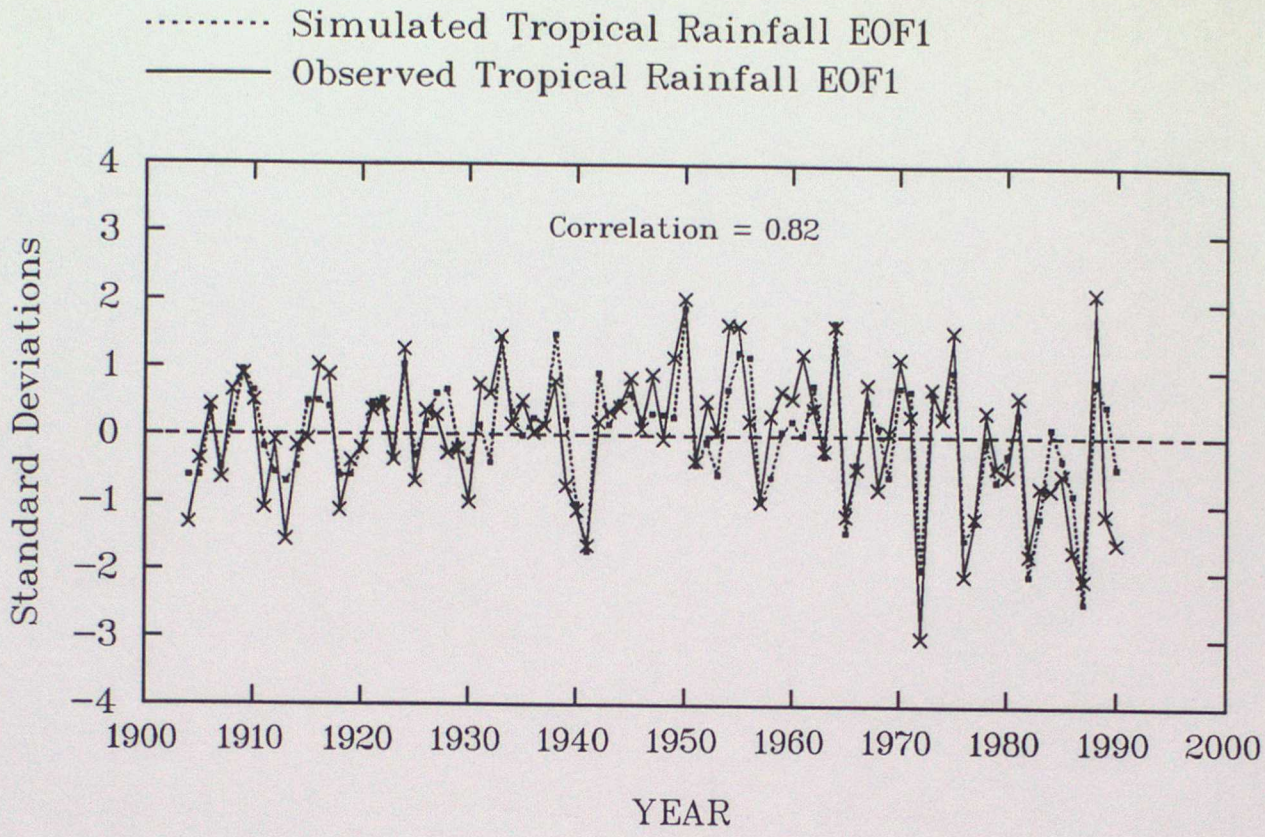

FIG. 9 Observed JAS time coefficients 1904-90 of tropical rainfall EOF1 (solid line with crosses, see Fig. 1b for the EOF pattern) and simulated EOF1 values using a multiple regression on three SST EOFs measured in JAS (see text for regression equation).

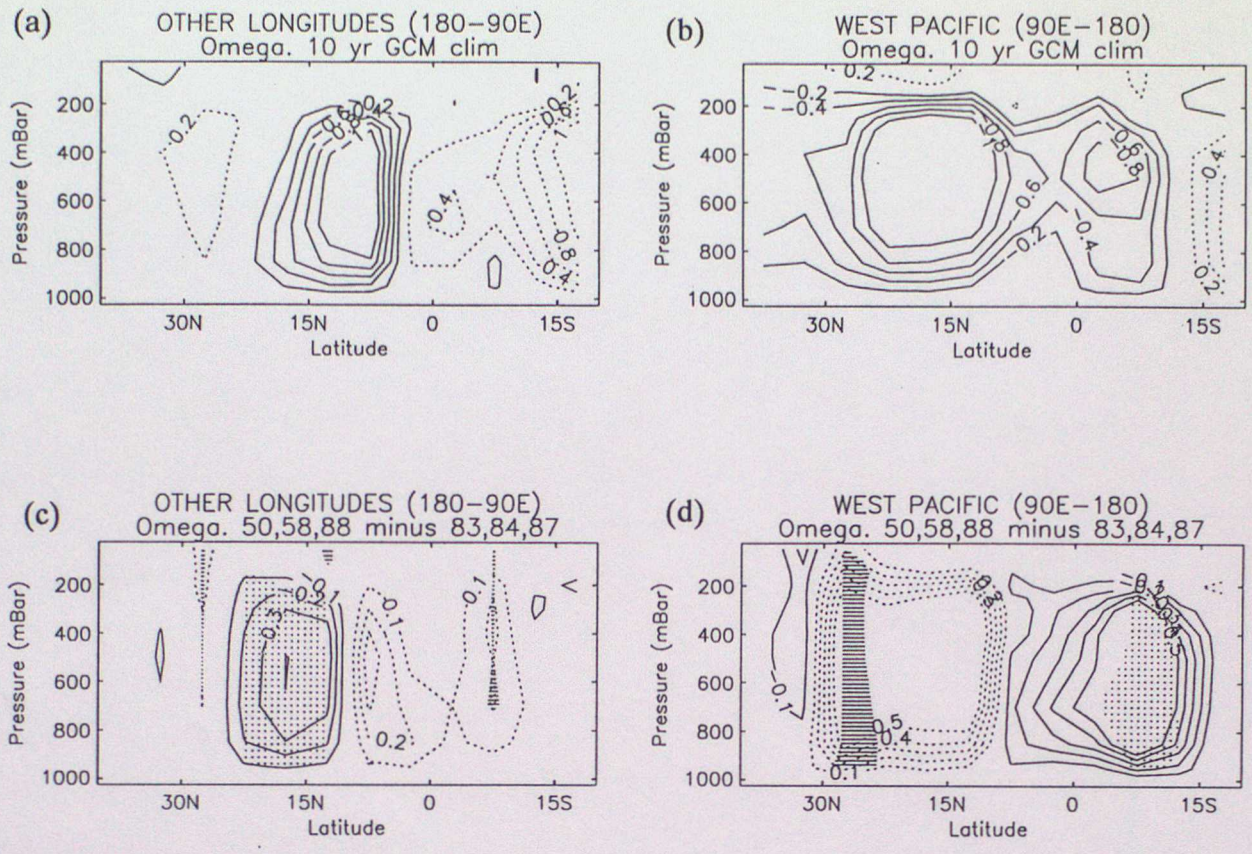

FIG. 10 Latitude/pressure cross-sections from 40°N to 20°S of JAS vertical motion (omega, ascent=negative) simulated by the GCM for (a) 10 year GCM climatology averaged over longitudes away from the western Pacific (90°E westward to 180), contours at +/-1,.8,.6,.4,.2, (Units are mb per hour), (b) as (a) but averaged over western Pacific longitudes (180 westward to 90°E, so part of the eastern Indian Ocean is also included, consistent with the GCM EOF pattern in Fig. 1a), (c) strongest negative tropic-wide oscillation years (50,58,88) minus strongest positive tropic-wide oscillation years (83,84,87) averaged over longitudes away from the western Pacific (90°E westward to 180), contours at +/-.5,.4,.3,.2,.1 and (d) as (c) but averaged over western Pacific longitudes (180 westward to 90°E) (Units are mb per hour). In (c) and (d), shading and hatching indicates negative and positive differences significant at the 10% level.

CLIMATE RESEARCH TECHNICAL NOTES

CRTN 1	Oct 1990	Estimates of the sensitivity of climate to vegetation changes using the Penman-Monteith equation. P R Rowntree
CRTN 2	Oct 1990	An ocean general circulation model of the Indian Ocean for hindcasting studies. D J Carrington
CRTN 3	Oct 1990	Simulation of the tropical diurnal cycle in a climate model. D P Rowell
CRTN 4	Oct 1990	Low frequency variability of the oceans. C K Folland, A Colman, D E Parker and A Bevan
CRTN 5	Dec 1990	A comparison of 11-level General Circulation Model Simulations with observations in the East Sahel. K Maskell
CRTN 6	Dec 1990	Climate Change Prediction. J F B Mitchell and Qing-cun Zeng
CRTN 7	Jan 1991	Deforestation of Amazonia - modelling the effects of albedo change. M F Mylne and P R Rowntree
CRTN 8	Jan 1991	The role of observations in climate prediction and research. D J Carson
CRTN 9	Mar 1991	The greenhouse effect and its likely consequences for climate change. D J Carson
CRTN 10	Apr 1991	Use of wind stresses from operational N.W.P. models to force an O.G.C.M. of the Indian Ocean. D J Carrington
CRTN 11	Jun 1991	A new daily Central England Temperature series, 1772-1991. D E Parker, T P Legg and C K Folland
CRTN 12	Jul 1991	Causes and predictability of Sahel rainfall variability. D P Rowell, C K Folland, K Maskell, J A Owen, M N Ward

CLIMATE RESEARCH TECHNICAL NOTES

CRTN 13	Jul 1991	Modelling changes in climate due to enhanced CO2, the role of atmospheric dynamics, cloud and moisture. C A Senior, J F B Mitchell, H Le Treut and Z-X Li
CRTN 14	Sep 1991	Sea temperature bucket models used to correct historical SST data in the Meteorological Office. C K Folland
CRTN 15	Aug 1991	Modelling climate change, and some potential effects on agriculture in the U.K. P R Rowntree, B A Callander and J Cochrane
CRTN 16	Aug 1991	The Boreal Forests and Climate G Thomas and P R Rowntree
CRTN 17	Aug 1991	Development of a Stratosphere-Troposphere Data Assimilation System. R Swinbank.
CRTN 18	Sep 1991	A study of asynchronous coupling using a simple climate model. M K Davey.
CRTN 19	Sep 1991	The Oceanic Carbon Cycle. N K Taylor
CRTN 20	Nov 1991	Worldwide ocean-atmosphere surface fields in Sahel wet and dry years using provisionally corrected surface wind data. M N Ward
CRTN 21	Dec 1991	Coupled tropical ocean global atmosphere models at the UKMO. M K Davey, C Gordon, S Ineson and S Lawrence
CRTN 22	Dec 1991	Empirical parameterisation of tropical ocean-atmosphere coupling. M Allen, M K Davey, D L T Anderson and P D Killworth
CRTN 23	Feb 1992	The temporal evolution of Equatorial Currents in the Indian Ocean D L T Anderson, D J Carrington, R A Corry and C Gordon
CRTN 24	Feb 1992	Stratospheric analyses provided by the U.K. Meteorological Office M J Bailey, A O'Neill and V D Pope

CLIMATE RESEARCH TECHNICAL NOTES

CRTN 25	Feb 1992	Modelling interannual variability in the Indian Ocean using momentum fluxes from the UKMO and ECMWF operational weather analyses. D L T Anderson and D J Carrington
CRTN 26	Mar 1992	A GCM simulation of the impact of Amazonian deforestation on climate using an improved canopy representation J Lean and P R Rowntree
CRTN 27	Mar 1992	The parameterization of rainfall interception in GCMs A J Dolman and D Gregory
CRTN 28	Jun 1992	Development of worldwide marine data eigenvectors since 1985 A W Colman
CRTN 29	Jun 1992	A tropical ocean model with reduced physics M K Davey
CRTN 30	Jun 1992	International Temperature Workshop, Boulder, Colorado, USA, 16 January 1992 Edited by D E Parker
CRTN 31	Jul 1992	Simulation of clear-sky outgoing longwave radiation over the oceans using operational analyses A Slingo and M J Webb
CRTN 32	Sep 1992	A prediction of the transient response of climate J M Murphy
CRTN 33	Nov 1992	LEPS scores for assessing climate model simulations and long-range forecasts. C K Folland
CRTN 34	Jan 1993	Stratospheric Data Assimilation System Guide Editer: R Swinbank
CRTN 35	Mar 1993	A Stratosphere-Troposphere Data Assimilation System R Swinbank and A O'Neill
CRTN 36	Mar 1993	Validation of hydrological schemes for climate models against catchment data. P R Rowntree and J Lean

CLIMATE RESEARCH TECHNICAL NOTES

CRTN 37	Apr 1993	Modelling of palaeoclimates: Examples from the recent past J F B Mitchell
CRTN 38	May 1993	A simulation of seasonality in ENSO forecast skill M K Davey, D L T Anderson and S Lawrence
CRTN 39	Jul 1993	ENSO Prediction experiments using a simple ocean-atmosphere model D-H Wu, D L T Anderson and M K Davey
CRTN 40	Sep 1993	Diagnosis of dynamic sea-surface and sea-level changes from the Cox ocean model J M Gregory
CRTN 41	Sep 1993	Seasonal variations of the clear-sky greenhouse effect: the role of changes in atmospheric temperatures and humidities M J Webb, A Slingo and G L Stephens
CRTN 42	Nov 1993	Sea-level changes under increasing atmospheric CO_2 in a transient coupled ocean-atmosphere GCM experiment. J M Gregory
CRTN 43	Dec 1993	Global and regional patterns of climate change: recent predictions for the Arctic P R Rowntree
CRTN 44	Feb 1994	The effect of changing horizontal diffusion in the atmospheric version of the unified climate model C D Hall and R A Stratton
CRTN 45	Mar 1994	Simulation of El-Niño/Southern Oscillation like variability in a global AOGCM and its response to CO_2 increase. S F B Tett
CRTN 46	Apr 1994	Global data required for monitoring climate change. D E Parker and C K Folland
CRTN 47	May 1994	Seasonal uptake of anthropogenic CO_2 in an ocean general circulation model. N K Taylor